Ultrasonics 93 (2019) 139–144

Contents lists available at ScienceDirect

Ultrasonics

journal homepage: www.elsevier.com/locate/ultras

Ultrasonic torsion welding of ageing-resistant Al/CFRP joints: Properties, microstructure and joint formation

Florian Staab*, Frank Balle

University of Freiburg, Walter and Ingeborg Herrmann Professorship for Engineering of Functional Materials (EFM), Department for Sustainable Systems Engineering (INATECH), Faculty of Engineering, 79110 Freiburg, Germany

ARTICLE INFO

2010 MSC:
00-01
99-00

Keywords:
Ultrasonic welding
Aluminum
Fiber reinforced thermoplastics
Ageing resistant
Hybrid structures
Multi-material-design

ABSTRACT

Ultrasonic metal welding is a promising process for joining light metals with fiber-reinforced thermoplastics. The technique is characterized by high reproducibility, short process times, low energy input, no additional filler materials and finally the possibility of extensive process data logging. With this process, dissimilar aerospace materials are ultrasonically welded and the applied process parameters are optimized by statistical methods. A prediction of ageing resistance is possible by the evaluation of the electrical resistivity of the multi-material-joints. With the help of detailed process parameter recording and microscopic investigations, the bonding mechanism of hybrid AA5024/(GF-)CF-PEEK joints is explained and the kinematics of bonding formation is presented in detail.

1. Introduction and motivation

Limited fossil fuels, political and ecological pressures or the aim for increased economic efficiency are the drivers behind a lightweight design. As a direct result, the application of fiber-reinforced polymers (FRP) is continuously increasing, especially in the aviation industry but also in automotive engineering. Since the substitution of monolithic materials as a direct tool for lightweight components has its limits, the structural weight of a component is determined not only by the materials selection but also by the joining technique to enable entire multi-material structures. Riveting is a historically established and currently most widespread joining process in aircraft engineering. The disadvantages of this process are particularly clear in case of carbon fiber reinforced polymers (CFRP): Load-bearing carbon fibers are destroyed during drilling, the mechanical load-bearing capacity of the components is significantly reduced and in order to compensate for this, a thickening of the joining areas is necessary. This fact and additional weight in the form of rivets contradicts the concept of lightweight. Long process times and difficult quality assurance motivate research of alternative joining processes. In addition to adhesive bonding [1,2], friction spot joining [3] and ultrasonic assisted joining processes like friction stir welding [4] or clinching [5], ultrasonic metal welding is a promising approach for joining aerospace materials such as aluminium, titanium alloys and fiber-reinforced thermoplastics. The process is used for similar joints in the packaging and textile industry as ultrasonic polymer welding [6] and as ultrasonic metal welding for example to close airbag capsules or to join cable harnesses in automotive engineering [7]. These two related technologies differ in the direction of oscillation of the welding tool, the so-called sonotrode. While in ultrasonic polymer welding the sonotrode oscillates perpendicular to the joining area [8,9], in ultrasonic metal welding a sonotrode oscillation in the joining plane is transferred to the interface of the single-overlapped joining partner. Although the industrial application focuses on joining similar materials, scientific approaches investigate joining materials of different types, such as metal with glasses, ceramics or light metals with fiber-reinforced thermoplastics [10–14].

The process is characterized by a high degree of process data control and therefore possibilities for automation, low process times and moderate process temperatures. Ultrasonic metal welding is the method of choice for joining lightweight materials such as aluminium or titanium alloys with fiber-reinforced thermoplastics. In both technologies, the polymer layer is melted on the surface and an adhesive bond is formed between the two joining partners. But only in case if the sonotrode oscillates in the plane of the joining surface the load-bearing fibers, which are not destroyed by the process, are directly bonded to the metallic surface [15]. The focus of the research is to transfer

* Corresponding author.
E-mail address: staab@inatech.uni-freiburg.de (F. Staab).
URL: http://www.inatech.uni-freiburg.de (F. Staab).

https://doi.org/10.1016/j.ultras.2018.11.006
Received 17 September 2018; Received in revised form 14 November 2018; Accepted 16 November 2018
Available online 22 November 2018
0041-624X/ © 2018 Elsevier B.V. All rights reserved.

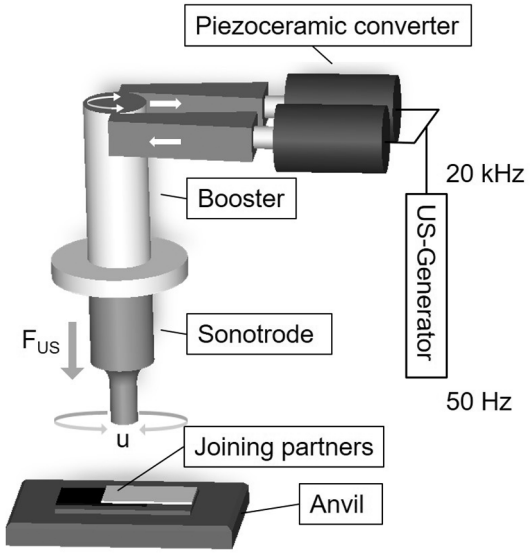

Fig. 1. Schematic diagram of an ultrasonic torsion welding system: W_{US}: Welding Energy, F_{US}: Welding Force, u: Oscillation Amplitude.

ultrasonic welding to further material combinations, to characterize the welds mechanically, physically and chemically and to investigate the transferability to industrial applications.

2. Ultrasonic torsion welding

Ultrasonic welding in its metal variant is a friction based joining technology characterised by a static pressure F_{US} combined with a superimposed ultrasonic oscillation of defined amplitude (u). The general structure of an ultrasonic welding system is shown in Fig. 1. The generator converts the mains voltage with a frequency of 50 Hz into an electrical oscillation of 20 kHz. Piezoceramic converters translate the electrical into a mechanical vibration of the same ultrasonic frequency. The connected booster stabilizes this oscillation and can additionally, increase or decrease the needed oscillation amplitude. The actual welding tool, the so-called sonotrode, finally introduces the vibrations into the upper joining partner. The technology of ultrasonic torsion welding, a subspecies of metal welding, offers some interesting advantages compared to the spot welding technology. Due to the different kind of vibration transmission, up to four piezoceramic converter can be implemented into the oscillatory system, which allows a higher welding power of up to 14 kW and therefore e.g. shorter welding times. The architecture of the system facilitates access to the joining zone, which allows more degrees of freedom in the design of the hybrid components to be joined.

3. Experimental setup

A TSP 3000 ultrasonic torsion welding system from Telsonic Ultrasonics (Switzerland) was chosen for this study. It is characterized by a maximum welding force F_{US} of 3000 N and a maximum generator output of 6500 W. The system has been extended by a custom-made specimen clamping to fix a pre-defined sample geometry during the welding process in order to perform reproducible welding experiments. In addition, a separate measurement data acquisition system was implemented, which records several further process parameters online during the joining process and enables a more detailed interpretation of the process. Since, due to geometric relationships, the oscillation amplitude of the sonotrode in ultrasonic torsion welding depends on the radial distance to the center line or zero position, a ring shaped sonotrode tip was selected. In contrast to a full-surface sonotrode tip, this reduces the amplitude variance and applies a welding force only to areas of the joining zone where there is also a sufficient displacement amplitude. The inner diameter is 10 mm, the outer diameter 15 mm, which results in a coupling surface of about 100 mm^2. The maximum oscillation amplitude of the selected sonotrode is 50 μm. The monotonic properties of the joints were evaluated by tensile shear tests, whose clamping device compensates the single overlap of the joints. To reduce the amount of welding experiments and to include the interaction of parameters, suitable process parameters were determined via design of experiments (DoE). In order to carry out temperature measurements, three grooves in the thickness of the thermocouples (Type J, thickness 1 mm) were milled into the organic sheets. To reduce the falsifying influence of molten and flowing polymers on temperature measurement, the channels were then sealed with PEEK-based granulate.

4. Base materials

The materials investigated in the research project were drafted directly from aircraft production and are provided by the project partners AIRBUS (Bremen, Germany) and Composite Technology Center GmbH (Stade, Germany). The joints presented in this paper were welded from the aluminium alloys AA2198 and AA5024 (selected mechanical properties in Table 1) and organic sheets from the fiber-reinforced thermoplastic matrix polyether ether ketone (PEEK) and polyphenylene sulfide (PPS), see Table 2. In addition to six layers of carbon fibers in satin 1/4 fabric (fiber volume ratio $V_f \approx 55\%$), the CFRP joining-partner has a glass fiber surface ply to prevent electrochemical contact corrosion and thus ensure ageing resistance. Both joining partners were cut from sheet material to the defined sample geometry (Al: 70 × 25 mm, CFRP: 70 × 30 mm) and the metallic partner was milled to a thickness of 1.2 mm. The thickness of all CFRP sheets was 1.8 mm. Before the welding process, all sheets were cleaned by ethanol from residues in an ultrasonic bath. No further chemical or mechanical surface treatment was applied so far.

5. Results and discussion

5.1. Mechanical and electrical joint properties

In order to determine suitable process parameters consisting of welding energy W_{US}, welding force F_{US} and oscillation amplitude u, a parameter space of defined size was implemented around a predefined center point. The lower and upper limits of the investigated parameter were as followed: Welding Force F_{US} 200–400 N; Welding Energy W_{US} 3500–4600 Ws; Oscillation Amplitude u: 36.5–50 μm. The result of the 'central composite design circumscribed' (CCC) is exemplaric shown as a 3D response surface plot at a constant welding energy of 4300 Ws in Fig. 2. The ultimate lap shear force for AA5024/(GF)-CF-PEEK joint's was predicted by the software Modde with its optimizer function. The calculated value was validated in subsequent separate welding experiments with 8310 N. The plot allows to determine a unique parameter triple, which provides a local maximum for the tensile shear strength in

Table 1
Selected mechanical properties of the aluminum wrought alloys AA2198 and AA5024.

Sheet materials	Treatment/condition	Young's modulus [GPa]	Yield strength [MPa]	UTS [MPa]	Ultimate elongation A_{50} [%]
AA2198	T851	77.4 ± 0.3	420 ± 5	475 ± 6	10.6 ± 0.7
AA5024	H116	72.8 ± 0.6	315 ± 4	395 ± 5	12.4 ± 1.2

Table 2
Selected mechanical and thermal properties of the carbon fiber reinforced thermoplastics CF-PEEK and CF-PPS.

Carbon composites	Young's modulus in 1-direction E_{11} [GPa]	UTS in 1-direction [MPa]	Thermal properties [16,17]	Melting Point [°C]	Decomposition temperature [°C]
CF-PEEK	60.1 ± 0.4	850 ± 28	PEEK	340	>550
CF-PPS	58.4 ± 0.3	750 ± 24	PPS	285	>450

the investigated parameter space.

Fig. 3 shows a comparison of the ultimate lap shear forces for all realized hybrid joints. Welds containing the aluminium alloy AA2198 show significantly poorer properties. Measuring the hardness of the aluminium in the region of the joining zone via a ZwickRoell ZHU 250 system (averaged for 6 points within 3 mm distance to the sonotrode tip) before and after the joining process results in a 56% reduction in Brinell hardness (HBW 2.5/62.5) from 147±5 HBW to 65±4 HBW due to the heat input during ultrasonic welding and corresponding local softening. According to [18], a heat treatment in which the US joining process is embedded are recommended to increase the bond strength when precipitation hardened aluminum alloys are involved. Before ultrasonic welding, the aluminium sheets were solution annealed at 500 °C for 60 min and the hybrid joint finally artificially aged at 180 °C for 20 h in a Nabertherm l40/12/p320 furnace. This heat treatment not only considerably increased the achievable tensile force (+25% for AA2198/(GF)-CF-PEEK; +88% for AA2198/(GF)-CF-PPS), the standard deviations within the sample quantity were significantly reduced (from ±910 to ±550 N for AA2198/(GF)-CF-PEEK; from ±832 to ±390 N for AA2198/(GF)-CF-PPS). For work hardenable aluminum alloys like AA5024, this kind of heat treatment is not needed. Suitable process parameters and resulting shear forces for all investigated joints are summarized in Table 3.

To study the bonding mechanisms, cross sections through the joining zone were prepared (Fig. 4). The high tensile shear forces can be explained by a microstructural comparison of the joining zone (Fig. 4a, left) and areas outside (Fig. 4b, right). In the area of the sonotrode tip, the polymer layer between the glass fiber ply and the polymer surface layer is completely melted and displaced. The aluminium sheet shows a local direct contact with the undamaged glass fibers and is pressed into the interstices between the single glass fibers by strong plastic deformation of the aluminum at the hybrid interface. This leads to an additional mechanical interlock and the adhesive bond is extended by a cohesive component in this area.

To verify the electrical insulating properties of the glass fiber surface ply after a welding process, the electric transition resistance of both, specimen with and without glass fiber fabric manufactured with identical welding parameters (4300 Ws, 300 N, 40 µm), was measured using a Hameg Instruments LCR-Meter in a fourpoint probes method, see sketch in Fig. 5. In order to ensure adequate electrical contacting of the transition structure and thus to reduce deviations in the measured value caused by this, the composites were drilled at corresponding positions and the cables were electrically connected by a thin silver layer. Due to the increase in electrical resistance from $R = 8,8\,\Omega \pm 2,7\,\Omega$ for joints without glass fiber surfacy ply to $R = 405\,M\Omega \pm 81\,M\Omega$ for hybrid welds with insulatory glass fiber plies, the ultrasonic torsion welded joining area in these hybrid systems can be considered as electrical insulating. Since all of the 12 glass-fiber-insulated composites examined show an electrically insulating transition structure in this measurement, it can be assumed that the joining process has no adverse effects on the glass fiber surface ply and thus a direct contact between carbon fiber and aluminum can be excluded and therefore no electrochemical aging of the hybrid joints is expected.

5.2. Interpretation of process and bonding kinematics

Fig. 6 shows the characteristic power-time course of an ultrasonic torsion welding process for Al/CFRP-joints. The power W is applied by the generator of the ultrasonic welding machine during the process in order to keep the sonotrode vibrating at a defined oscillation amplitude u and during superimposed welding force F_{US}. The course of the curve can be divided into three characteristic sections: a sharp peak at the beginning of the process in which the sonotrode starts to oscillate (1), the middle section with an unsteady increase and a smooth drop around the process' maximum value of the welding power (2) and a concluding section in which the course of the curve is very unsteady and moves against a limit value under a periodic fluctuation (3–4). Distinctive characteristic values of the curve progression are reproducible and

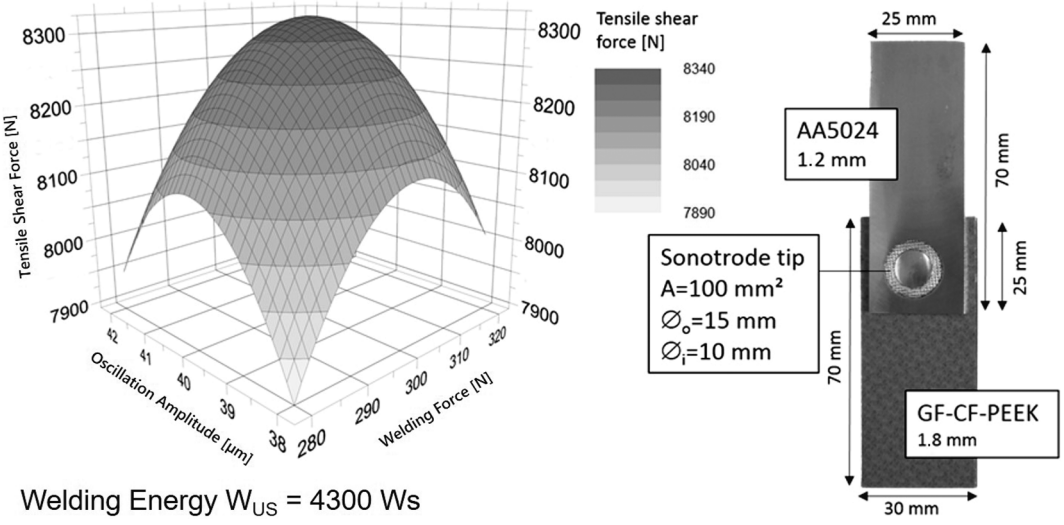

Fig. 2. Left: Calculated surface plot of ultimate lap shear force in dependency of welding parameters Welding Force and Oscillation Amplitude; Right: Specimen Geometry [13].

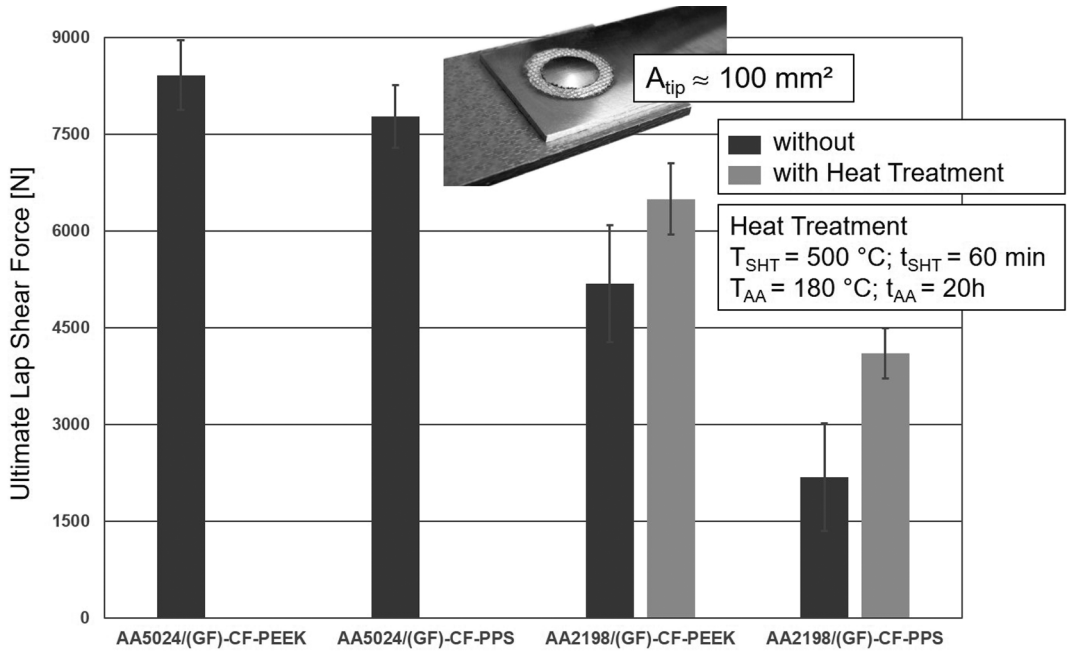

Fig. 3. Experimentally determined ultimate lap shear forces for different hybrid joints. AA2198-based joints were optionally subjected to heat treatment before and after the joining process corresponding to T6 conditions.

Table 3
Suitable process parameters (calculated via Modde 7) and measured ultimate lap shear forces. (*after heat treatment).

	Welding energy W_{US} [Ws]	Welding force F_{US} [N]	Oscillation amplitude u [µm]	Maximum tensile shear force [N]
AA5024/(GF)-CF-PEEK	4300	300	40	8310 ± 540
AA5024/(GF)-CF-PPS	3650	220	44	7900 ± 490
AA2198/(GF)-CF-PEEK	4600	380	40	6490* ± 550
AA2198/(GF)-CF-PPS	4400	340	48	4100* ± 390

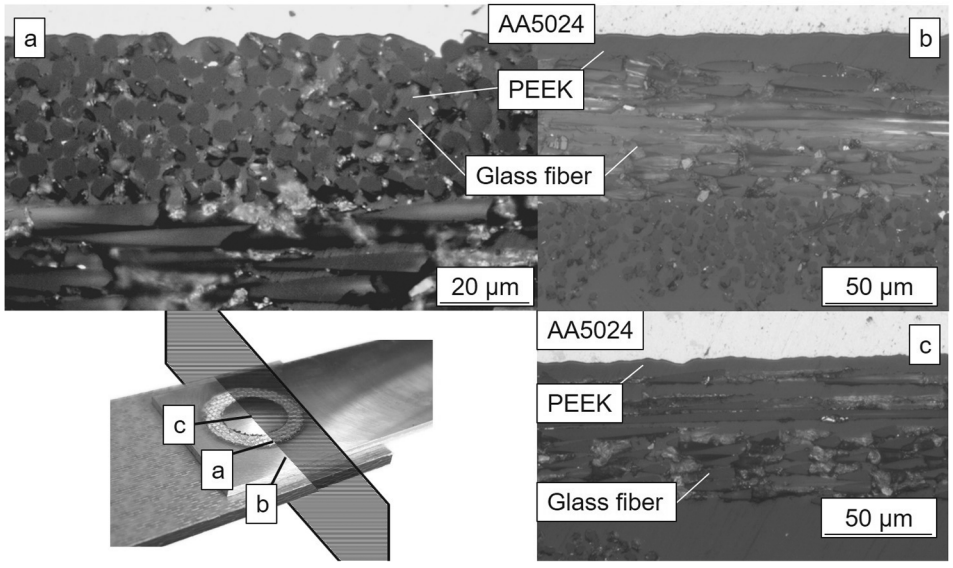

Fig. 4. Cross sections of joining zone (a), outside areas (b) and areas in the middle of the ring (c).

depend primarily on the physical and mechanical material properties of both joining partners.

Due to plastic deformation and a relative movement of both joining partners, heat is generated and introduced into the joining zone. The temperature in the area of the joining zone was measured for three characteristic positions: 1. directly underneath the tip surface, 2. in the centre of the ring, i.e. without direct oscillation introduced by the sonotrode and 3. in a range with a distance of 5 mm outside of the tip

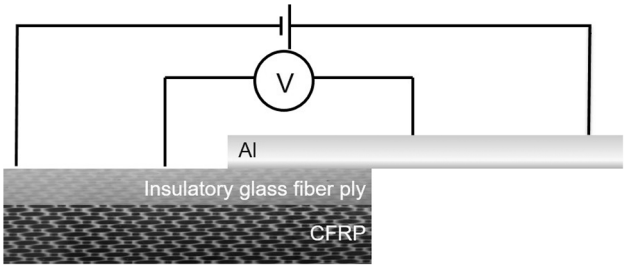

Fig. 5. Schematic arrangement for measuring the electrical transition resistance of an ultrasonic welded hybrid joint.

surface. As it is to be expected, the temperature in the direct oscillation area (Thermocouple 1) increases the fastest. After a welding time of about 1.5 s, the melting temperature of PEEK is exceeded here. The thermoplastic matrix is molten and displaced by the welding force applied by the sonotrode, both inwards and outwards. The temperature inside (Thermocouple 2) and outside (Thermocouple 3) of the joining zone follows T1 at a time interval and because heat can be dissipated faster to the outside, the melting temperature of PEEK ($T_{S,PEEK}$ = 340 °C) is reached at T3 but not significantly exceeded. At no time in the welding process the decomposition temperature of PEEK ($T_{D,PEEK}$ >550 °C) is reached, so a lasting thermal damage of the matrix can be excluded. A comparison of the P- and T1-course shows that the transition from range 2 to 3 takes place when the melting temperature of PEEK in the joining zone is exceeded. Seemingly, alternating melting and displacement processes in the thermoplastic matrix lead to a fluctuating material resistance, which explains the transition to the unsteady curve of power.

In order to analyse the kinematics of bond formation more precisely, stop-action welding experiments were carried out. For this purpose, four characteristic periods were defined in the Power-Time-diagram and the energy input up to these points was determined and averaged for six welds: Point 1 directly after the first oscillations of the sonotrode (after a welding time t_{US} ≈0.2 s), point 2 in the range of the maximum welding power (t_{US} ≈1.0 s), point 3 at which the melting temperature of PEEK is exceeded (t_{US} ≈1.8 s) and after completion of a conventional welding (t_{US} ≈5.2 s). For further evaluation of these points, both the weld path and, if possible, the ultimate lap shear force of the bond were determined and both joining partners and the joining zone were microscopically examined. After a welding process that has been completed at points 1 and 2, no joint closure can be observed. The characteristic impression of the welding tool's knurled pattern can be seen on the surface of the metallic joining partner, with which the weld path of about 0.06 mm can be explained. The surface of the organic sheet is only subject to mechanical abrasion of the uppermost polymer layer. A sufficient energy input to establish a first connection is introduced at point 3. The first melting of the remaining thermoplastic polymer took place here, which was identified as residues after the tensile shear test on the metallic joining partner (Fig. 7a). At this time, the hybrid bond is purely adhesive and shows the tensile shear force of 2200 N. The cross section through the joining zone of the organic sheet shows that the polymer layer was completely removed up to the glass fiber cover layer at this point (Fig. 8b). An increase in the weld path of only 0.01 mm does not indicate a cohesive proportion of the bond yet. Only from this point on, the polymer melt between the individual glass fibers takes place. Due to plastic deformation and the applied welding force, aluminium is now yield into the resulting gaps, which leads to a mechanical interlock between metal and fibers and a significant increase in the welding path to a final distance of 0.27 mm. The ultimate lap shear force increases from 2200 N (Point 3) to 8310 N (Point 4). This can also be seen in the distinctly different appearance of the fracture surfaces: not only polymer residues are present on the metallic joining partner, but the failure of the joint now occurs in the glass fiber surface ply, which is torn out of the organic sheet around the joining zone (Fig. 7b).

6. Conclusions

Based on statistical experimental design, hybrid joints out of aluminium alloy AA5024 and GF/CF-PEEK were realized with a tensile shear strength of 83 ± 5 MPa calculated with a sonotrode tip area of 100 mm². A metallographic characterization of the joining zone shows adhesive (between aluminium and polymer) as well as cohesive (between aluminium and glass fibers) components of bonding. The kinematics of the bond formation were described and analyzed on the basis of evolution spots during ultrasonic torsion welding in the joining process, which were defined by evaluating the Power-Time diagram. The analysis showed that only when a welding time of 1.8 s is exceeded does the composition of the bond types change from a solely adhesive bond in the joining zone to adhesive and cohesive components.

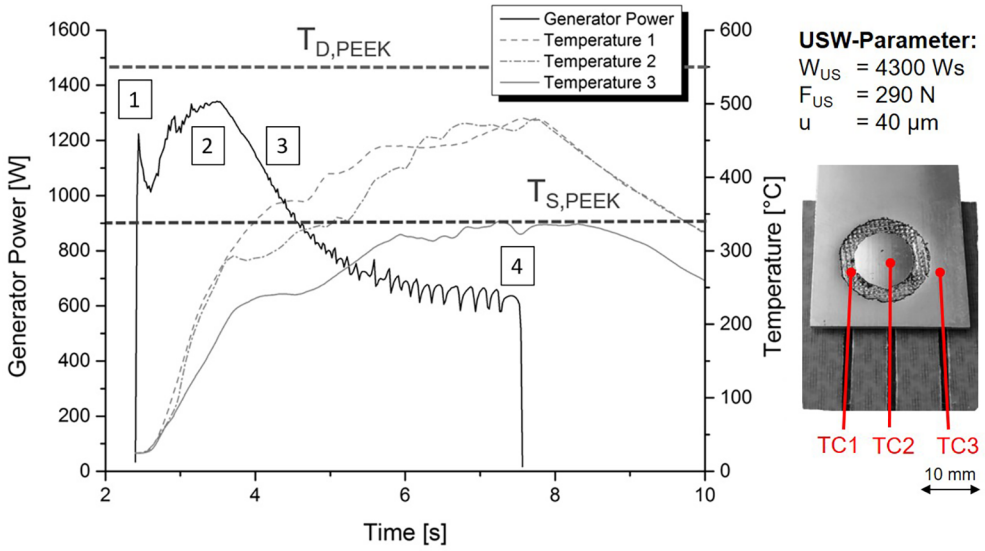

Fig. 6. Characteristic Power-Temperature-Time-Course for an AA5024/(GF)-CF-PEEK ultrasonic welding process, welding temperatures for three positions and characteristic points in the P-T-t course.

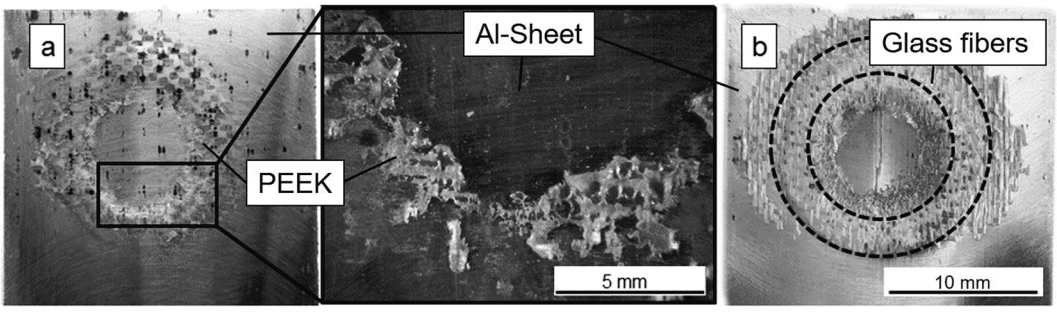

Fig. 7. Fracture surfaces of an AA5024/(GF)-CF-PEEK joint at point 3 (a) and 4 (b) in Fig. 6.

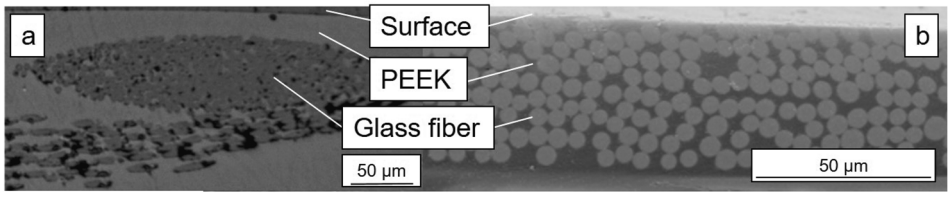

Fig. 8. Cross section of glass fiber surface ply as base material (a) and at point 3 (b).

Acknowledgments

The authors would like to thank the German Research Foundation (DFG) for the financial support in the framework of project BA4073/9-1, as well as the industrial partners from AIRBUS/CTC Bremen, Hamburg and Stade, especially Johannes Born, Carsten Rowedder, Thomas Kruse and Freerk Syassen for the support of materials and the fruitful discussions.

References

[1] G. Scarselli, C. Corcione, F. Nicassio, A. Maffezzoli, Int. J. Adhes. Adhes. 75 (2017) 174–180, https://doi.org/10.1016/j.ijadhadh.2017.03.012.
[2] H. Wang, X. Hao, H. Zhou, D. Li, L. Hua, J. Adhes. Sci. Technol. 30 (2016) 1842–1857, https://doi.org/10.1080/01694243.2016.1168338.
[3] N.M. André, S.M. Goushegir, J.F. dos Santos, L.B. Canto, S.T. Amancio-Filho, Compos. Part B: Eng. 94 (2016) 197–208, https://doi.org/10.1016/j.compositesb.2016.03.011.
[4] Z. Liu, S. Ji, X. Meng, Int. J. Adv. Manuf. Technol. 97 (2018) 4127–4136, https://doi.org/10.1007/s00170-018-2255-8.
[5] F. Heßeln, M.C. Wanner, Adv. Mater. Res. 966–967 (2014) 641–650, https://doi.org/10.4028/www.scientific.net/amr.966-967.641.
[6] P.D.L. Staff, Handbook of Plastics Joining, Elsevier S&T, 1997 https://www.ebook.de/de/product/15162798/pdl_staff_handbook_of_plastics_joining.html .
[7] J. Gould, Weld. J. 91 (2012) 23–34.
[8] F. Lionetto, M.N. Morillas, S. Pappadà, G. Buccoliero, I.F. Villegas, A. Maffezzoli, Compos. Part A: Appl. Sci. Manuf. 104 (2018) 32–40, https://doi.org/10.1016/j.compositesa.2017.10.021.
[9] I.F. Villegas, R. van Moorleghem, Compos. Part A: Appl. Sci. Manuf. 109 (2018) 75–83, https://doi.org/10.1016/j.compositesa.2018.02.022.
[10] J. Magin, F. Balle, Material wiss. Werkstofftech. 45 (2014) 1072–1083, https://doi.org/10.1002/mawe.201400355.
[11] F. Balle, G. Wagner, D. Eifler, Adv. Eng. Mater. 11 (2009) 35–39, https://doi.org/10.1002/adem.200800271.
[12] C. Born, G. Wagner, D. Eifler, Adv. Eng. Mater. 8 (2006) 816–820, https://doi.org/10.1002/adem.200600083.
[13] F. Staab, F. Balle, J. Born, Key Eng. Mater. 742 (2017) 395–400, https://doi.org/10.4028/www.scientific.net/kem.742.395.
[14] S. Krüger, G. Wagner, D. Eifler, Adv. Eng. Mater. 6 (2004) 157–159, https://doi.org/10.1002/adem.200300539.
[15] G. Wagner, F. Balle, D. Eifler, Adv. Eng. Mater. 15 (2013) 792–803, https://doi.org/10.1002/adem.201300043.
[16] V.K. Thakur, M.K. Thakur, R.K. Gupta, Hybrid Polymer Composite Materials, Elsevier Science, 2017 https://www.ebook.de/de/product/29287491/hybrid_polymer_composite_materials.html .
[17] G.W. Ehrenstein, G. Riedel, P. Trawiel, Thermal Analysis of Plastics – Theory and Practice, Hanser Publishers, 2004.
[18] F. Balle, S. Huxhold, S. Emrich, G. Wagner, M. Kopnarski, D. Eifler, Adv. Eng. Mater. 15 (2012) 837–845, https://doi.org/10.1002/adem.201200301.